Optically pure, water-stable metallo-helical 'flexicate' assemblies with antibiotic activity

Suzanne E. Howson,[a] Albert Bolhuis,[b] Viktor Brabec,[c] Guy J. Clarkson,[a] Jaroslav Malina,[c] Alison Rodger,[a] Peter Scott*[a]

[a] Department of Chemistry, University of Warwick, Gibbet Hill Road, Coventry, CV4 7AL, UK.

[b] Department of Pharmacy and Pharmacology, University of Bath, Bath, BA2 7AY, UK.

[c] Institute of Biophysics, Academy of Sciences of the Czech Republic, Královopolská 135, CZ-61265 Brno, Czech Republic.

* Author to whom correspondence and requests for materials should be addressed.

Email address: peter.scott@warwick.ac.uk

Abstract

The helicates – chiral assemblies of two or more metal atoms linked by short or relatively rigid multidentate organic ligands – may be regarded as non-peptide mimetics of α-helices because they are of comparable size and have shown some relevant biological activity. Unfortunately, these beautiful helical compounds have remained difficult to use in the medicinal arena, because they either contain mixtures of isomers, cannot be optimised for specific purposes, are insoluble or are too difficult to synthesise. Instead, we have now prepared thermodynamically stable single enantiomers of monometallic units connected together by organic linkers. This highly adaptable self-assembly approach enables the rapid preparation of ranges of water-stable helicate-like compounds with high stereochemical purity. One such iron(II) 'flexicate' system exhibits specific interactions with DNA, promising antimicrobial activity against a Gram-positive bacterium (methicillin-resistant *Staphylococcus aureus*, MRSA252) but also, unusually, a Gram-negative bacterium (*Escherichia coli*, MC4100), and low toxicity towards a non-mammalian model organism (*C. elegans*).

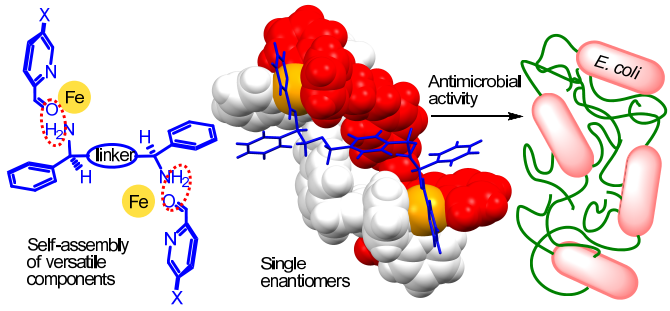

Protein α-helices perform structural and signalling roles in Nature through interactions with nucleic acids, other peptides and membranes. As a result of this biochemistry, synthetic α-helices have a role as motifs in the development of drug molecules.[1-4] However, since they are challenging to synthesise on a reasonable scale and have lability to proteases (leading to unfavourable pharmacokinetics)[2] there is a substantial effort to design and synthesise organic peptidomimetic and non-peptide mimetic systems.[5-9]

The helicates[10-18] commonly comprise a chiral assembly of three ditopic bidentate organic ligands BA–AB around two metal centres, for example Fig. 1(a). Some examples are of a similar diameter to α-helices (*ca* 1.2 nm) and there is hope that these coordination complexes could have therapeutic and medical diagnostic applications as non-peptide mimetics. Indeed synthetic and biophysical studies towards this general aim are being carried out by groups worldwide,[19-21] but notably by Hannon and co-workers.[14,22-34] Nevertheless, the practical impact of this type of research in medicinal chemistry will be limited unless certain criteria can be achieved. Helicates must be: (i) optically pure and non-racemising for use in human systems; (ii) soluble and stable in water to enable studies in biological media; (iii) readily available on a practical scale; and (iv) synthetically flexible so that drug-like properties can be designed or optimised.[35] The closest approach to achievement of these criteria was made very recently with an Fe(II) helicate bearing arginine-derived substituents;[22] this water soluble compound was available in both enantiomerically-enriched forms, but as a single example on a small scale after a lengthy synthesis.

In our view the core of the problem is the helicate approach itself, whereby the helicity at each octahedral metal M in Fig. 1 (a) is mechanically coupled using relatively stiff or short ligands B-A—A-B leading to an overall chiral structure.[35] Our approach

has been to avoid this design element and to develop methods by which thermodynamically stable single enantiomers of *monometallic* compounds may be produced from simple optically pure ligands at labile metals,[36,37] and then to connect together such stereochemically "pre-programmed" units using linkers of our choice. This has not hitherto been achieved because of the profound difficulty in synthesising stereochemically pure monometallic complexes. Here we report the successful outcome of this strategy; two series of optically pure, water-stable, functionalised, readily available bimetallic architectures. The conventional helicate approach (mechanical coupling between metal centres) is not used here and the new assemblies can be designed to have different degrees of flexibility. In recognition of these distinctions we use the term *flexicate* for these helicate-like compounds. In addition to specific interactions with DNA, they show very promising antimicrobial activity towards methicillin-resistant *Staphylococcus aureus* (MRSA) and *Escherichia coli* (*E. Coli*) alongside low toxicity to the non-mammalian model organism *Caenorhabditis elegans* (*C. elegans*).

Results

Synthesis, Self-Assembly and Characterisation

Alkylation of two equivalents of (*R*)-2-phenylglycinol with one equivalent of α,α′-dibromo-*p*-xylene gave the optically pure diamine **1** [Fig. 1 (b)]. The reaction of **1** with 2-pyridinecarboxaldehyde and $Fe(ClO_4)_2 \cdot 6H_2O$ in the proportions 3:6:2 led to the immediate formation of an intense purple solution. NMR analysis indicated a very complex mixture containing various metal/ligand assemblies but on heating at 85°C for 24 hours (or microwaving for 20 min) complete conversion was observed to a *single* bimetallic flexicate Δ_{Fe},R_C-$[Fe_2\mathbf{L}^{\mathbf{1a}}{}_3][ClO_4]_4$. Crystallisation gave chemically, optically

and diastereomerically pure Δ_{Fe},R_C-[Fe_2**L**$^{1a}{}_3$][ClO_4]$_4$ [Fig. 1 (b)]. The flexicate with opposite helicity (Λ_{Fe}) was prepared similarly starting from (*S*)-2-phenylglycinol. The Zn(II) flexicate Δ_{Zn},R_C-[Zn_2**L**$^{1a}{}_3$][ClO_4]$_4$ self-assembled within minutes at ambient temperature. We note that Telfer and Kuroda reported non-helical halide-bridged bimetallics when related L-valinol derivatives of *meta*-xylene were used.[38,39]

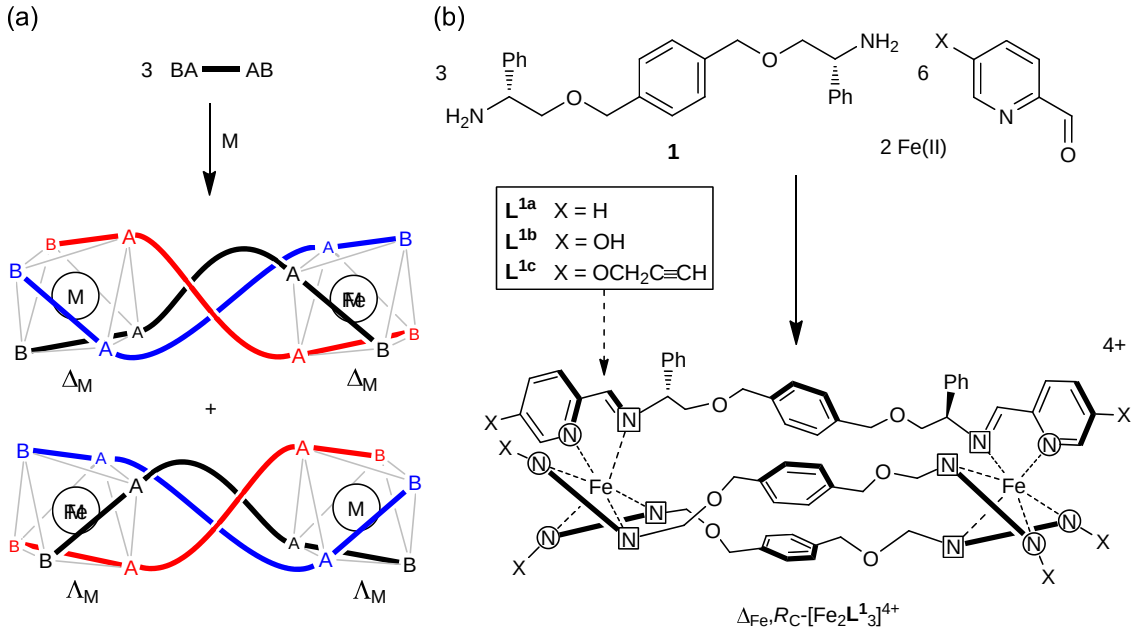

Figure 1 | Self assembly of helical bimetallics: (a) a *helicate* synthesis in which a relatively rigid achiral ligand causes the helicity of two metal centres to be mechanically coupled, leading to a mixture of *P* (Δ_M,Δ_M) and *M* (Λ_M,Λ_M) compounds; (b) a *flexicate* synthesis in which the stereochemistries of the two metals are predetermined independently, leading to in this case the diastereomerically pure (Δ_{Fe},Δ_{Fe}) compound R_C-[Fe_2**L**$^1{}_3$][ClO_4]$_4$ despite the flexible diether linker. Only one ligand is shown in full. In the others, N atoms in circles and squares are from pyridine and imine units respectively.

The ^{1}H NMR spectrum of the Fe(II) flexicate Δ_{Fe},R_C-[Fe_2**L**$^{1a}{}_3$][ClO_4]$_4$ (Fig. 2) shows the high and unequivocal diastereomeric purity (*d.r.* > 200:1) evident from, for example, the absence of peaks in the imine region (8 – 10 ppm) that are higher than the ^{13}C satellites of the main resonance at 8.96 ppm. The Zn(II) flexicate spectrum is

similar. The flexicates gave excellent electrospray mass spectra with strong peaks for the tetracationic molecular ions.

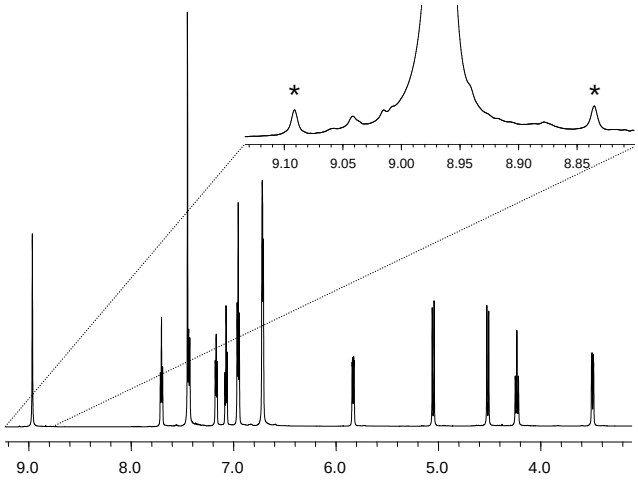

Figure 2 | ^{1}H NMR spectrum of Δ_{Fe},R_C-[Fe_2**L**$^{\mathbf{1a}}{}_3$][ClO_4]$_4$ in CD_3CN (700 MHz). ^{13}C satellites for the imine CH unit indicated * represent 0.5% of the sample each and are larger than any impurity resonances.

Isomorphous crystals of the Fe(II) and Zn(II) flexicates, Δ_{Fe},R_C-[Fe_2**L**$^{\mathbf{1a}}{}_3$][ClO_4]$_4$ and Δ_{Zn},R_C-[Zn_2**L**$^{\mathbf{1a}}{}_3$][ClO_4]$_4$, were grown and the Zn(II) structure was fully refined (chiral space group $P3_112$). The triple-stranded tetracation assembly is shown in Fig. 3 (see Supplementary Fig. S1 online for structural figure with probability ellipsoids, CCDC reference number 847378). Both metal centres have *fac*,Δ_{Zn} configurations and are connected by three diether linkers. Each metal centre is approximately octahedral with a mean average Zn–N bond length of 2.17 Å.[37] At the metal centres, each of the three pyridine units form an optimal parallel-displaced π-stack with a phenyl unit on a neighbouring ligand.[37,40] The average angle between the mean planes of the pyridine and phenyl rings is 4.9° (range 3.0 – 7.6°) and the average centroid-centroid distance is 3.65 Å (range 3.62 – 3.71 Å).

The presence of six sp^3 centres per linker in the M(II) flexicates allows for many potential conformations, and while the ^{1}H NMR spectrum indicated an averaged C_3-

symmetry for the system in solution, the observed solid state structure has two distinct linker orientations. The ligands in red and green (Fig. 3) form a zig-zag chain between metal centres, while the ligand in blue (Fig. 3) traces an essentially linear route between the metal centres. Despite this, the overall assembly is only slightly "bent" along the nominal C_3 axis (see Supplementary Fig. S1 online for a detailed description of the linker orientations).

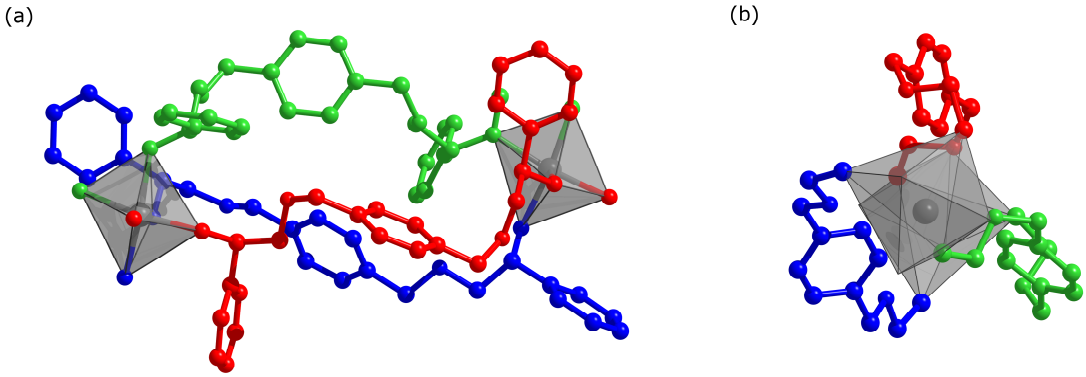

Figure 3 | Views of the structure of the cation unit in Δ_{Zn},R_C-$[Zn_2\mathbf{L}^{\mathbf{1a}}{}_3][ClO_4]_4{\cdot}2CH_3CN{\cdot}3H_2O{\cdot}½MeOH$ (CCDC reference number 847378) with H atoms omitted for clarity and coordination octahedra in grey: (a) the ligand in blue is essentially linear while those in red and green zig-zag between the coordination units; (b) the overall structure is nevertheless close to 3-fold axial symmetry (phenyl rings omitted for clarity).

The above structural study indicates that the optically and diastereomerically pure metal centres in Δ_{Fe},R_C-$[Fe_2\mathbf{L}^{\mathbf{1a}}{}_3][ClO_4]_4$ and Δ_{Zn},R_C-$[Zn_2\mathbf{L}^{\mathbf{1a}}{}_3][ClO_4]_4$ will be able to tolerate the presence of unusual linker groups, and in particular those which would normally be expected to lead to product mixtures containing for example achiral *mesocates*.[41] As a robust test of this idea, and also to create an architecture with the aminoalcohol functionality at the structure termini, we treated **2**[42] (Fig. 4) in acetonitrile with appropriate equivalents of $Fe(ClO_4)_2{\cdot}6H_2O$ and (*S*)-(–)-α-methylbenzylamine as before. The ^{1}H NMR spectra of both the crude and purified products, dark pink Δ_{Fe},S_C-

$[Fe_2\mathbf{L}^{\mathbf{2a}}{}_3][ClO_4]_4$, revealed that the self-assembly reaction is highly diastereoselective (see Supplementary Fig. S2 online) and also that there is excellent thermodynamic chemoselectivity for the $[M_2L_3]^{4+}$ structure (Fig. 4). The Zn(II) flexicate Δ_{Zn},S_C-$[Zn_2\mathbf{L}^{\mathbf{2a}}{}_3][ClO_4]_4$ self-assembled within minutes at ambient temperature, and has similar NMR spectra.

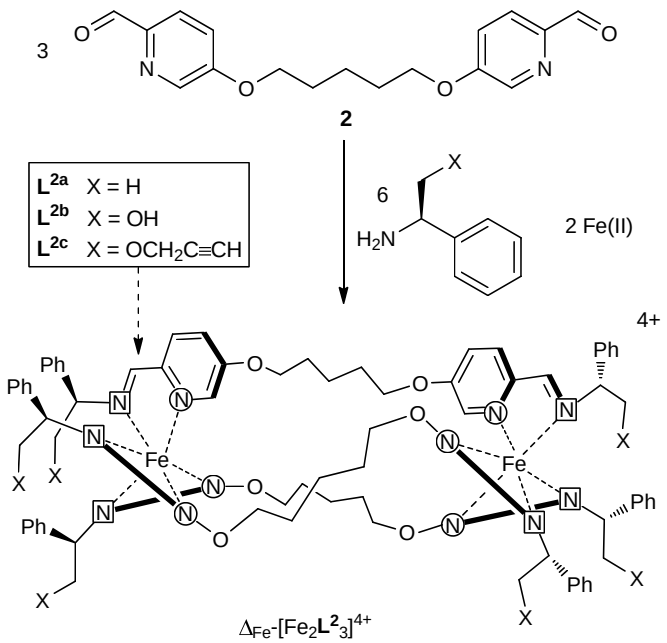

Figure 4 | Self assembly of diastereomerically pure Δ_{Fe}-$[Fe_2\mathbf{L}^{\mathbf{2}}{}_3][ClO_4]_4$ flexicate systems with highly flexible C_5 linkers and with, in contrast to the structures depcited in Figure 1(b), with aminoalcohol functionality at the structure termini. Only one ligand is shown in full. In the others, N atoms in circles and squares are from pyridine and imine units respectively.

Functionalised derivatives of both the $\mathbf{L}^{\mathbf{1}}$ and $\mathbf{L}^{\mathbf{2}}$ series are readily available by variation of the pyridine and amine components respectively, and examples with hydroxyl and alkynyl substituents are shown in Figures 1 and 4. These and other examples have similar spectroscopic properties to the parent flexicates and have very high stereochemical purity. The alkyne flexicates Δ_{Fe},R_C-$[Fe_2\mathbf{L}^{\mathbf{1c}}{}_3][ClO_4]_4$ and Δ_{Fe},R_C-$[Fe_2\mathbf{L}^{\mathbf{2c}}{}_3][ClO_4]_4$ are versatile synthons in copper(I)-catalysed Huisgen 1,3-dipolar

cycloaddition (CuAAC) click reactions with organic azides, and we will report this chemistry in due course.

All the Fe(II) flexicates give excellent circular dichroism (CD) spectra with intense features spanning the whole UV-visible region as a result of π-π* and metal-ligand charge transfer transitions. The spectra of enantiomers were found to be equal and opposite (see Supplementary Fig. S3 online). In particular, the intense bisignate curves centred around 544 nm resulting from strong exciton coupling in the metal-ligand charge transfer transitions confirm the formation of non-racemic chiral metal centres. Comparison with the metal-ligand charge transfer bands in the CD spectra of the structurally similar Δ- and Λ-$[Fe(bpy)_3]^{2+}$ enantiomers confirms the configuration assignments as Δ_{Fe} for S_C-$\mathbf{L}^{\mathbf{2a}}$ and Λ_{Fe} for R_C-$\mathbf{L}^{\mathbf{2a}}$.[43,44] Such features are ideal for spectroscopic studies of, for example, DNA binding because of their intensity and their position well away from DNA-based absorptions. They are also highly sensitive to structural changes and would, for example, not be present in the event of decomposition of the flexicate.

Water-soluble chloride salts of both series, such as Δ_{Fe},R_C-$[Fe_2\mathbf{L}^{\mathbf{1a}}{}_3]Cl_4$ were prepared quantitatively using $FeCl_2$ as the metal source. These are spectroscopically indistinguishable from the ClO_4^- salts described above (see Supplementary Fig. S4 online). Critically, CD spectra of solutions of these flexicates in water showed little change over lengthy storage periods with no indications of stereochemical leakage. Even at pH 1.5, Δ_{Fe},R_C-$[Fe_2\mathbf{L}^{\mathbf{1a}}{}_3]Cl_4$ suffered only *ca* 8% decomposition over 10 days while the more flexibly-linked Δ_{Fe},S_C-$[Fe_2\mathbf{L}^{\mathbf{2a}}{}_3]Cl_4$ has a $t_{½}$ of 9.6 hours. The flexicates are also stable in the presence of nucleic acids, and we have studied DNA binding by various means.

DNA Binding

Apparent binding constants (K_{app}) to DNA, calculated from ethidium bromide displacement experiments, reveal that all flexicates exhibit higher binding affinities for the double-stranded poly(dA-dT)$_2$ DNA than for natural calf-thymus (ct) DNA and poly(dG-dC)$_2$ (Table 1). This indicates selectivity for the AT-rich sequence. The Δ_{Fe}/Λ_{Fe}-[Fe$_2$**L**$^{\mathbf{1a}}{}_3$]Cl$_4$ flexicates exhibit significantly higher binding affinities in all cases compared to the Δ_{Fe}/Λ_{Fe}-[Fe$_2$**L**$^{\mathbf{2a,b}}{}_3$]Cl$_4$ flexicates. In cases where there is a significant enantiomeric difference, the Λ_{Fe} enantiomer always has a higher binding affinity compared to the Δ_{Fe} enantiomer. The binding constants are nearly double those reported for related $[M_2L_3]^{4+}$ complexes (M = Fe^{II}, Ru^{II}).[26,27]

Linear dichroism (LD) spectroscopy measures the difference in absorption of light polarised parallel and perpendicular to the orientation axis of the molecule [LD =$A_{\parallel}$ - $A_{\perp}$]. Laminar flow is used in LD spectroscopy in order to orient long molecules such as DNA predominantly in one direction [Fig. 5 (a)]. The linear dichroism (LD) spectra of all [Fe$_2$**L**$^{\boldsymbol{n}}{}_3$]Cl$_4$ flexicates (*n* = **1a**, **2a**, **2b**) in the absence of ct-DNA exhibit no LD signals indicating that, as expected, the Fe(II) flexicates alone are too small to align in the flow in the cell. With the two [Fe$_2$**L**$^{\mathbf{1a}}{}_3$]Cl$_4$ enantiomers, the addition of ct-DNA caused changes in the LD spectra consistent with alignment and binding in a specific orientation (see Supplementary Fig. S5 and S6 online). The induced LD signals are more intense for the Λ_{Fe} enantiomer. In contrast, the [Fe$_2$**L**$^{\mathbf{2a,b}}{}_3$]Cl$_4$ flexicates all displayed very little indication of alignment. Presumably only electrostatic interactions with the anionic DNA backbone are present for this particular series of flexicates.

Molecules can align on a stretched film (for example polyethylene) with their long axis oriented along the stretch direction thus allowing the predominant polarisation of transitions at given wavelengths to be determined. The long axis and short axis

transitions in the flow LD spectrum of the $[Fe_2\mathbf{L}^{\mathbf{1a}}{}_3]Cl_4$ flexicates have been characterised from film LD data (see Supplementary Fig. S7 online). Both the long axis (575 nm) and short axis (360 nm) transitions have positive signals in the flow LD spectrum of the flexicates with DNA. As a result, and since LD is proportional to $(3\cos^2\alpha\text{-}1)$ where α is the angle between the DNA helix axis and the transition moment, the flexicates must be oriented in such a way that the angles between the flow axis and the long and short axes are both less than 54.7°. The differences in signal intensities between the long axis polarised transitions at 575 nm and the short axis polarised transitions at 360 nm are greater in the LD spectra compared to in the UV-Vis absorbance spectra (see Supplementary Fig. S7 online). Therefore the flexicate must be oriented on the DNA so that 54.7° > short axis angle > long axis angle, relative to the flow axis [Fig. 5 (b)]. In order for this to hold, the flexicate must be oriented at approximately 40 – 45° to the flow axis. This angle is the same as the angle of the grooves in DNA relative to the helix/flow axis [Fig. 5 (a)], and therefore suggests that the Δ_{Fe}/Λ_{Fe}-$[Fe_2\mathbf{L}^{\mathbf{1a}}{}_3]Cl_4$ flexicates target the grooves of DNA. Given that this flexicate has a diameter of *ca* 1.2 nm – similar to that of a typical α-helix – we can assume major groove binding [Fig. 5 (c)]; the minor groove is too narrow.

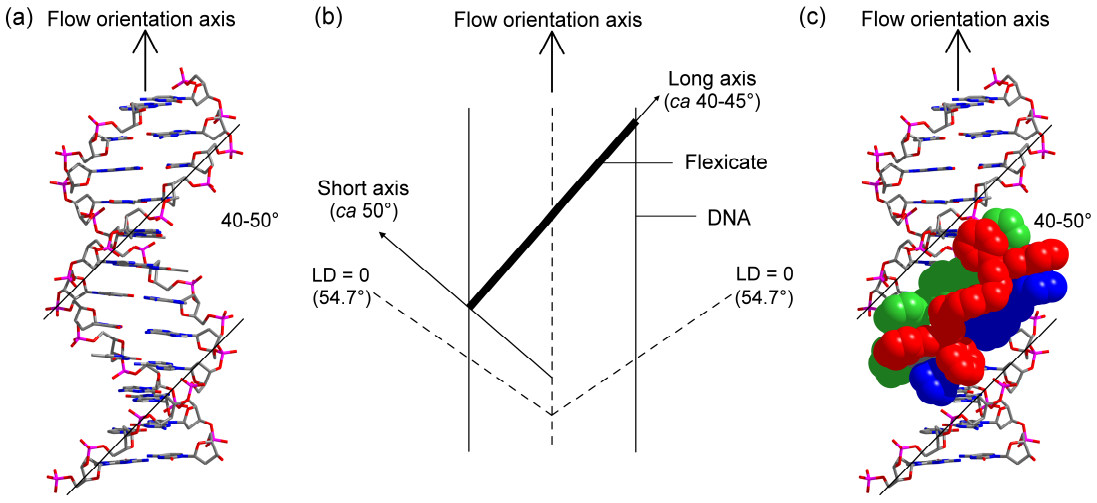

Figure 5 | Derivation of the binding angle of the flexicate relative to the DNA helix/flow orientation axis: (a) major groove highlighted in B-DNA; (b) schematic diagram showing the derived orientation of the flexicate on DNA; (c) schematic diagram showing the flexicate sitting in the major groove of B-DNA. All labelled angles are relative to the flow orientation axis.

The melting temperature (T_m) of DNA is an effective measure of its thermal stability and is defined as the temperature at which half of the DNA strands are in the double-helical state and half have unwound into a 'random coil' state. The changes in melting temperature (ΔT_m) of ct-DNA in the presence of the $[Fe_2\mathbf{L}^{n}{}_3]Cl_4$ flexicates (*n* = **1a**, **2a**, **2b**) are listed in Table 1 and show that both enantiomers of $[Fe_2\mathbf{L}^{\mathbf{1a}}{}_3]Cl_4$ stabilise the ct-DNA causing an increase in its melting temperature. The Λ_{Fe} enantiomer exhibits a higher stabilising effect on the ct-DNA than the Δ_{Fe} enantiomer. The $[Fe_2\mathbf{L}^{\mathbf{2}}{}_3]Cl_4$ series of flexicates have no effect on the melting temperature of ct-DNA. These results fit with the conclusions made from the spectroscopic measurements previously described, *i.e.* the $[Fe_2\mathbf{L}^{\mathbf{1a}}{}_3]Cl_4$ flexicates bind strongly in a specific mode whereas the $[Fe_2\mathbf{L}^{\mathbf{2a,b}}{}_3]Cl_4$ flexicates only exhibit electrostatic interactions.

Antimicrobial Activity and Toxicity

The antimicrobial activity of enantiomers of $[Fe_2\mathbf{L}^{\mathbf{1a}}{}_3]Cl_4$, $[Fe_2\mathbf{L}^{\mathbf{2a}}{}_3]Cl_4$ and $[Fe_2\mathbf{L}^{\mathbf{2b}}{}_3]Cl_4$ were carried out against the Gram-negative bacterium *Escherichia coli* (MC4100) and the Gram-positive bacterium methicillin-resistant *Staphylococcus aureus* (MRSA252). The latter is resistant to several antibiotics, including penicillin, methicillin, ciprofloxacin, and erythromycin.[45] The tested flexicates displayed antimicrobial activity against both types of bacteria with their minimum inhibitory concentrations (MIC) as low as 4 μg/ml (*ca* 2 μM) against *E. coli* (Table 1). While antimicrobial activity of certain coordination compounds was noted some time ago,[46] this result is remarkable

since coordination compounds often have low potency against, in particular, Gram-negative bacteria,[24,47] possibly as a result of the protective lipopolysaccharide-containing outer membrane.[48]

This preliminary MIC data indicates two trends in the antimicrobial activity of the flexicates: (i) the systems with the less polar ligands ($\mathbf{L^{1a}} < \mathbf{L^{2a}} < \mathbf{L^{2b}}$) are the more effective; (ii) the Λ_{Fe} enantiomers are more effective than the Δ_{Fe} enantiomers.

Toxicity tests were carried out for the most biologically active flexicates – the $[Fe_2\mathbf{L^{1a}}_3]Cl_4$ enantiomers – on nematode *Caenorhabditis elegans*. The use of *C. elegans* as a simple and convenient model to test for toxicity is justified since it shares several biological features with higher eukaryotes[49] and is considered a good indicator for the toxicity therein.[50] The worms were exposed to different concentrations of the tested flexicates for 24 hours and the LC50 values were determined (Table 1). The $[Fe_2\mathbf{L^{1a}}_3]Cl_4$ enantiomers had LC50 values of 408 μg/ml (Λ) and 500 μg/ml (Δ), making them significantly less toxic than ethidium bromide (LC50 = 145 μg/ml). Considering the high potency of these flexicates as antimicrobial agents, their relatively low toxicity in *C. elegans* is highly promising. The LC50 value of one of the least biologically active flexicates, Λ_{Fe},S_C-$[Fe_2\mathbf{L^{2b}}_3]Cl_4$, was also measured (Table 1). The higher toxicity of this flexicate compared to the $[Fe_2\mathbf{L^{1a}}_3]Cl_4$ enantiomers suggests there is no relationship between toxicity and the antimicrobial potency.

Discussion

The metallo-helical assemblies described here arise from a different approach – linking together of pre-programmed optically pure monometallic units – which does not rely on the helicate concept of mechanically-coupled metal centres and allows quite free variation of the linkers and end groups. The π-stacking interactions present in these

flexicates, enhanced by metal coordination, contribute substantially to the excellent observed diastereoselectivity, and the accompanying hydrophobic effect imparts unusually high aqueous stability. Overall we believe that the flexicates satisfy the practical criteria which will allow translation from the chemistry lab to the clinic through biological studies. Early investigations in this direction are highly promising: the flexicates are amenable to biophysical studies, and differences in DNA binding constants between classes of flexicates are traced to major-groove binding for one class and simple electrostatic binding for another. The antibiotic properties are also dependent on structure and helicity, and the activity against the Gram-negative strain of *E.coli* MC4100 is particularly notable alongside the modest toxicity to *C. elegans*.

Perhaps most importantly however, the sheer practicality of this approach will allow us to explore this fascinating region of chemical space much more readily than has been possible hitherto, and if drug candidates are identified they are much more likely to be available in a form that could reach the clinic.

Methods

Key procedures are detailed below. Full experimental details for the synthesis of all new compounds, including procedures and characterisation, are given in the Supplementary Information. Protocols for the biophysical studies are also given in the Supplementary Information.

Synthesis of Λ_{Fe},S_C-[$Fe_2L^{1a}_3$]Cl_4

2-Pyridinecarboxaldehyde (0.28 g, 2.66 mmol, 6.0 eq.) and (*S*,*S*)-1,4-bis{(2-amino-2-phenylethoxy)methyl}benzene (**1**) (0.50 g, 1.33 mmol, 3.0 eq.) were dissolved in methanol (50 ml) and were stirred for 2 hours at ambient temperature. Anhydrous iron(II) chloride (0.11 g, 0.89 mmol, 2.0 eq.) was added as a solid and the solution turned intense purple in colour as the solid dissolved. The solution was stirred under reflux (80°C) for 24 hours. After cooling, the solvent was removed under reduced pressure to leave a purple solid, which was dried *in vacuo*. Yield = 0.85 g, 0.44 mmol, 100%.

Antimicrobial experiments

The bacterial strains used were *Escherichia coli* MC4100 and *Staphylococcus aureus* MRSA252 (see Supplementary Information online). Strains were maintained on Luria-Bertani (LB) broth (Fisher) or Brain Heart Infusion (BHI) broth (Fisher). Mueller-Hinton (MH; Fisher) broth was used to test sensitivity to antibiotics. The minimal inhibitory concentration (MIC) values of the flexicates were determined with a macrobroth dilution method (see Supplementary Information online). Stock solutions of all flexicates were made in 70% ethanol at a concentration of 10 mg/ml. These were diluted to appropriate concentrations in 3 ml of MH broth containing 105 cells per ml.

The cultures were incubated for 18 hours at 37°C and then scored for growth. The lowest concentration at which no growth was observed was defined as the MIC.

Analysis of toxicity in *Caenorhabditis elegans*

C. elegans Bristol (N2) nematodes were maintained on nematode growth medium, using *E. coli* OP50 as a source of food. Nematodes were age-synchronised (see Supplementary Information online), and between 20 and 30 L4-stage nematodes were placed in each well of a 24-well plate. The nematodes were exposed to different concentrations of the test flexicates for 24 hours, in a total volume of 1 mL M9 buffer (3 g/L KH_2PO_4, 6 g/L Na_2HPO_4, 5 g/L NaCl and 0.25 g/L $MgSO_4 \cdot 7H_2O$). Ethidium bromide was used as a control, and all tests were carried out in duplicate. Observations were carried out using a standard dissecting microscope; nematodes were scored as dead when they lost their normal sigmoidal shape and failed to move in response to agitation of the medium or gentle touch with a platinum wire. The LC50 (concentration that kills 50% of the nematodes) was determined for each flexicate tested.

Acknowledgements

We thank the EPSRC and the University of Warwick for financial support. We thank the EPSRC National Crystallography Service (University of Southampton, UK) for data collection.

Author Contributions

S.E.H. synthesised the compounds, carried out the spectroscopic studies, analysed data and drafted the paper; A.B. designed and performed the antimicrobial and toxicity

studies; V.B. and J.M. designed and performed the ethidium bromide displacement experiments and the DNA melting studies; G.J.C. solved and refined the X-ray crystal data; A.R. designed the linear dichroism studies and assisted with analysis of the resulting data; P.S. conceived and directed the project, analysed data and wrote the paper.

Figure Legends & Tables

Figure 1 | Self assembly of helical bimetallics: (a) a *helicate* synthesis in which a relatively rigid achiral ligand causes the helicity of two metal centres to be mechanically coupled, leading to a mixture of *P* (Δ_M,Δ_M) and *M* (Λ_M,Λ_M) compounds; (b) a *flexicate* synthesis in which the stereochemistries of the two metals are predetermined independently, leading to in this case the diastereomerically pure (Δ_{Fe},Δ_{Fe}) compound R_C-[Fe_2**L**$^{\mathbf{1}}{}_3$][ClO_4]$_4$ despite the flexible diether linker. Only one ligand is shown in full. In the others, N atoms in circles and squares are from pyridine and imine units respectively.

Figure 2 | ^{1}H NMR spectrum of Δ_{Fe},R_C-[Fe_2**L**$^{\mathbf{1a}}{}_3$][ClO_4]$_4$ in CD_3CN (700 MHz). ^{13}C satellites for the imine CH unit indicated * represent 0.5% of the sample each and are larger than any impurity resonances.

Figure 3 | Views of the structure of the cation unit in Δ_{Zn},R_C-[Zn_2**L**$^{\mathbf{1a}}{}_3$][ClO_4]$_4$·2CH_3CN·3H_2O·½MeOH (CCDC reference number 847378) with H atoms omitted for clarity and coordination octahedra in grey: (a) the ligand in blue is essentially linear while those in red and green zig-zag between the coordination units; (b) the overall structure is nevertheless close to 3-fold axial symmetry (phenyl rings omitted for clarity).

Figure 4 | Self assembly of diastereomerically pure Δ_{Fe}-[Fe_2**L**$^{\mathbf{2}}{}_3$][ClO_4]$_4$ flexicate systems with highly flexible C_5 linkers and with, in contrast to the structures depcited in Figure 1(b), with aminoalcohol functionality at the structure termini. Only one ligand is shown in full. In the others, N atoms in circles and squares are from pyridine and imine units respectively.

Figure 5 | Derivation of the binding angle of the flexicate relative to the DNA helix/flow orientation axis: (a) major groove highlighted in B-DNA; (b) schematic diagram showing the derived orientation of the flexicate on DNA; (c) schematic diagram showing the flexicate sitting in the major groove of B-DNA. All labelled angles are relative to the flow orientation axis.

Flexicate	Apparent binding constants, K_{app} (× 10^6 M^{-1})			ΔT_m (°C) of ct-DNA (DNA base:flexicate)		MIC (μg/ml)		LC50 for *C. elegans* (μg/ml)
	ct-DNA	poly $(dA\text{-}dT)_2$	poly $(dG\text{-}dC)_2$	20:1	10:1	*S. aureus* (Gram +)	*E. coli* (Gram -)	
Λ_{Fe},S_C-[Fe_2**L**$^{1a}{}_3$]Cl_4	110	212	108	6.8	12.9	8	4	408
Δ_{Fe},R_C-[Fe_2**L**$^{1a}{}_3$]Cl_4	111	210	83	4.9	8.9	8	8	500
Λ_{Fe},R_C-[Fe_2**L**$^{2a}{}_3$]Cl_4	56	124	37	0.0	-0.1	64	32	-
Δ_{Fe},S_C-[Fe_2**L**^{2a}]$_3Cl_4$	45	65	29	0.0	-0.2	64	>128	-
Λ_{Fe},S_C-[Fe_2**L**$^{2b}{}_3$]Cl_4	56	134	46	-0.1	-0.1	>128	>128	339
Δ_{Fe},R_C-[Fe_2**L**$^{2b}{}_3$]Cl_4	50	80	46	0.0	-0.1	>128	>128	-

Table 1 | DNA binding, antimicrobial and toxicity data for the flexicates.

References

1. Huang, Y., Huang, J. & Chen, Y. Alpha-helical cationic antimicrobial peptides: relationships of structure and function. *Protein Cell* **1**, 143-152 (2010).
2. Hancock, R. E. W. & Sahl, H.-G. Antimicrobial and host-defense peptides as new anti-infective therapeutic strategies. *Nat. Biotechnol.* **24**, 1551-1557 (2006).
3. Zasloff, M. Antimicrobial peptides of multicellular organisms. *Nature* **415**, 389-395 (2002).
4. Tossi, A., Sandri, L. & Giangaspero, A. Amphipathic, alpha-helical antimicrobial peptides. *Biopolymers* **55**, 4-30 (2000).
5. Boyle, A. L. & Woolfson, D. N. De novo designed peptides for biological applications. *Chem. Soc. Rev.* **40**, 4295-4306 (2011).
6. Cummings, C. G. & Hamilton, A. D. Disrupting protein-protein interactions with non-peptidic, small molecule alpha-helix mimetics. *Curr. Opin. Chem. Biol.* **14**, 341-346 (2010).
7. Haridas, V. From peptides to non-peptide alpha-helix inducers and mimetics. *Eur. J. Org. Chem.* **2009**, 5112-5128 (2009).
8. Grauer, A. & König, B. Peptidomimetics – A versatile route to biologically active compounds. *Eur. J. Org. Chem.* **2009**, 5099-5111 (2009).
9. Davis, J. M., Tsou, L. K. & Hamilton, A. D. Synthetic non-peptide mimetics of alpha-helices. *Chem. Soc. Rev.* **36**, 326-334 (2007).
10. Lehn, J.-M. *et al.* Spontaneous assembly of double-stranded helicates from oligobipyridine ligands and copper(I) cations: structure of an inorganic double helix. *Proc. Natl Acad. Sci. USA* **84**, 2565-2569 (1987).
11. He, C., Zhao, Y., Guo, D., Lin, Z. & Duan, C. Chirality transfer through helical motifs in coordination compounds. *Eur. J. Inorg. Chem.* **2007**, 3451-3463 (2007).
12. Piguet, C., Borkovec, M., Hamacek, J. & Zeckert, K. Strict self-assembly of polymetallic helicates: The concepts behind the semantics. *Coord. Chem. Rev.* **249**, 705-726 (2005).
13. Schalley, C. A., Lützen, A. & Albrecht, M. Approaching supramolecular functionality. *Chem. Eur. J.* **10**, 1072-1080 (2004).
14. Hannon, M. J. & Childs, L. J. Helices and helicates: Beautiful supramolecular motifs with emerging applications. *Supramol. Chem.* **16**, 7-22 (2004).
15. Albrecht, M. “Let's Twist Again” Double-stranded, triple-stranded, and circular helicates. *Chem. Rev.* **101**, 3457-3498 (2001).
16. Albrecht, M. How do they know? Influencing the relative stereochemistry of the complex units of dinuclear triple-stranded helicate-type complexes. *Chem. Eur. J.* **6**, 3485-3489 (2000).
17. Caulder, D. L. & Raymond, K. N. Supermolecules by design. *Acc. Chem. Res.* **32**, 975-982 (1999).
18. Constable, E. C. Oligopyridines as helicating ligands. *Tetrahedron* **48**, 10013-10059 (1992).
19. Glasson, C. R. K. *et al.* Microwave synthesis of a rare $[Ru_2L_3]^{4+}$ triple helicate and its interaction with DNA. *Chem. Eur. J.* **14**, 10535-10538 (2008).
20. Yu, H., Wang, X., Fu, M., Ren, J. & Qu, X. Chiral metallo-supramolecular complexes selectively recognize human telomeric G-quadruplex DNA. *Nucleic Acids Res.* **36**, 5695-5703 (2008).
21. Schoentjes, B. & Lehn, J.-M. Interaction of double-helical polynuclear copper(I) complexes with double-stranded DNA. *Helv. Chim. Acta* **78**, 1-12 (1995).

22. Cardo, L., Sadovnikova, V., Phongtongpasuk, S., Hodges, N. J. & Hannon, M. J. Arginine conjugates of metallo-supramolecular cylinders prescribe helicity and enhance DNA junction binding and cellular activity. *Chem. Commun.* **47**, 6575-6577 (2011).
23. Boer, D. R. *et al.* Self-assembly of functionalizable two-component 3D DNA arrays through the induced formation of DNA three-way-junction branch points by supramolecular cylinders. *Angew. Chem. Int. Ed.* **49**, 2336-2339 (2010).
24. Richards, A. D., Rodger, A., Hannon, M. J. & Bolhuis, A. Antimicrobial activity of an iron triple helicate. *Int. J. Antimicrob. Agents* **33**, 469-472 (2009).
25. Parajo, Y. *et al.* Effect of bridging ligand structure on the thermal stability and DNA binding properties of iron(II) triple helicates. *Dalton Trans.*, 4868-4874 (2009).
26. Malina, J., Hannon, M. J. & Brabec, V. DNA binding of dinuclear iron(II) metallosupramolecular cylinders. DNA unwinding and sequence preference. *Nucleic Acids Res.* **36**, 3630-3638 (2008).
27. Malina, J., Hannon, M. J. & Brabec, V. Interaction of dinuclear ruthenium(II) supramolecular cylinders with DNA: Sequence-specific binding, unwinding, and photocleavage. *Chem. Eur. J.* **14**, 10408-10414 (2008).
28. Hotze, A. C. G. *et al.* Supramolecular iron cylinder with unprecedented DNA binding is a potent cytostatic and apoptotic agent without exhibiting genotoxicity. *Chem. Biol.* **15**, 1258-1267 (2008).
29. Pascu, G. I., Hotze, A. C. G., Sanchez-Cano, C., Kariuki, B. M. & Hannon, M. J. Dinuclear ruthenium(II) triple-stranded helicates: Luminescent supramolecular cylinders that bind and coil DNA and exhibit activity against cancer cell lines. *Angew. Chem. Int. Ed.* **46**, 4374-4378 (2007).
30. Malina, J., Hannon, M. J. & Brabec, V. Recognition of DNA three-way junctions by metallosupramolecular cylinders: Gel electrophoresis studies. *Chem. Eur. J.* **13**, 3871-3877 (2007).
31. Oleksi, A. *et al.* Molecular recognition of a three-way DNA junction by a metallosupramolecular helicate. *Angew. Chem. Int. Ed.* **45**, 1227-1231 (2006).
32. Hotze, A. C. G., Kariuki, B. M. & Hannon, M. J. Dinuclear double-stranded metallosupramolecular ruthenium complexes: Potential anticancer drugs. *Angew. Chem. Int. Ed.* **45**, 4839-4842 (2006).
33. Meistermann, I. *et al.* Intramolecular DNA coiling mediated by metallosupramolecular cylinders: Differential binding of *P* and *M* helical enantiomers. *Proc. Nat. Acad. Sci. U.S.A.* **99**, 5069-5074 (2002).
34. Hannon, M. J. *et al.* Intramolecular DNA coiling mediated by a metallo-supramolecular cylinder. *Angew. Chem. Int. Ed.* **40**, 879-884 (2001).
35. Howson, S. E. & Scott, P. Approaches to the synthesis of optically pure helicates. *Dalton Trans.* **40**, 10268-10277 (2011).
36. Howson, S. E. *et al.* Self-assembling optically pure $Fe(A\text{-}B)_3$ chelates. *Chem. Commun.*, 1727-1729 (2009).
37. Howson, S. E. *et al.* Origins of stereoselectivity in optically pure phenylethaniminopyridine *tris*-chelates $M(NN')_3^{n+}$ (M = Mn, Fe, Co, Ni and Zn). *Dalton Trans.* **40**, 10416-10433 (2011).
38. Telfer, S. G., Kuroda, R. & Sato, T. Stereoselective formation of dinuclear complexes with anomalous CD spectra. *Chem. Commun.*, 1064-1065 (2003).
39. Telfer, S. G., Sato, T., Kuroda, R., Lefebvre, J. & Leznoff, D. B. Dinuclear complexes of chiral tetradentate pyridylimine ligands: Diastereoselectivity,

positive cooperativity, anion selectivity, ligand self-sorting based on chirality, and magnetism. *Inorg. Chem.* **43**, 421-429 (2004).
40. Hohenstein, E. G. & Sherrill, C. D. Effects of heteroatoms on aromatic π−π interactions: Benzene−pyridine and pyridine dimer. *J. Phys. Chem. A* **113**, 878-886 (2009).
41. Xu, J., Parac, T. N. & Raymond, K. N. *meso* Myths: What drives assembly of helical versus *meso*-[M_2L_3] clusters? *Angew. Chem. Int. Ed.* **38**, 2878-2882 (1999).
42. Bakunova, S. M. *et al.* Synthesis and antiprotozoal activity of pyridyl analogues of pentamidine. *J. Med. Chem.* **52**, 4657-4667 (2009).
43. Hidaka, J. & Douglas, B. E. Circular dichroism of coordination compounds. II. Some metal complexes of 2,2'-dipyridyl and 1,10-phenanthroline. *Inorg. Chem.* **3**, 1180-1184 (1964).
44. Ziegler, M. & von Zelewsky, A. Charge-transfer excited state properties of chiral transition metal coordination compounds studied by chiroptical spectroscopy. *Coord. Chem. Rev.* **177**, 257-300 (1998).
45. Holden, M. T. G. *et al.* Complete genomes of two clinical *Staphylococcus aureus* strains: Evidence for the rapid evolution of virulence and drug resistance. *Proc. Natl Acad. Sci. USA* **101**, 9786-9791 (2004).
46. Dwyer, F. P., Gyarfas, E. C., Rogers, W. P. & Koch, J. H. Biological activity of complex ions. *Nature* **170**, 190-191 (1952).
47. Bolhuis, A. *et al.* Antimicrobial activity of ruthenium-based intercalators. *Eur. J. Pharm. Sci.* **42**, 313-317 (2011).
48. Hancock, R. E. W. The bacterial outer membrane as a drug barrier. *Trends Microbiol.* **5**, 37-42 (1997).
49. Artal-Sanz, M., de Jong, L. & Tavernarakis, N. *Caenorhabditis elegans*: A versatile platform for drug discovery. *Biotechnol. J.* **1**, 1405-1418 (2006).
50. Leung, M. C. K. *et al. Caenorhabditis elegans*: An emerging model in biomedical and environmental toxicology. *Toxicol. Sci.* **106**, 5-28 (2008).